Structure-Thermal Conductivity Tentative Correlation for Hybrid Aerogels Based on Nanofibrillated Cellulose-Mesoporous Silica Nanocomposite

Dounia Bendahou[1,2], Abdelkader Bendahou[1], Bastien Seantier[1], Bénédicte Lebeau[3], Yves Grohens[1,*] and Hamid Kaddami[2,*]

[1]*University of Southern Brittany, Dupuy de Lôme Research Institute, FRE-CNRS 3744, BP 92116, 56321 Lorient Cedex, France*
[2]*Cadi Ayyad University, Faculty of Sciences and Technologies, Avenue Abdelkrim Elkhattabi, B.P. 549, Marrakech, Morocco*
[3]*University of Upper Alsace, Institute of Materials Science of Mulhouse (IS2M), 68057 Mulhouse Cedex, France*

Received May 26, 2017; Accepted November 11, 2017

ABSTRACT: Hybrid aerogels have been prepared by freeze-drying technique after mixing water dispersions of cellulose microfibers or cellulose nanofibers and silica (SiO_2) of type SBA-15 (2D-hexagonal). The prepared composites were characterized by different analysis techniques such as SEM, hot-filament, DMA, etc. These composites are compared to those previously prepared using nanozeolites (NZs) as mineral charge. The morphology studied by SEM indicated that both systems have different structures, i.e., individual fibers for cellulose microfibers WP-based aerogels and films for nanofibrillated cellulose NFC-based ones.... These differences seem to be driven by the charge of the particles, their aspect ratio and concentrations. These hybrid materials exhibit tunable thermal conductivity and mechanical properties. The thermal conductivity values range between ~18 to 28 $mW.m^{-1}.K^{-1}$ and confirm the superinsulation ability of these fibrous aerogels. Synergism on the thermal insulation properties and mechanical properties was shown by adjunction of mineral particles to both cellulose-based aerogels by reaching pore size lower than 100 nm. It significantly reduces the thermal conductivity of the hybrid aerogels as predicted by Knudsen *et al*. Furthermore, the addition of mineral fillers to aerogels based on cellulose microfibers induced a significant increase in stiffness.

KEYWORDS: Aerogels, cellulose microfibers WP, TEMPO-oxidized NFC, silica, lyophilization, porosity, superinsulation, mechanical properties

1 INTRODUCTION

Nanostructured aerogel materials (silica aerogel, polyurethane, cellulose, etc.) offer the properties of thermal superinsulation (thermal conductivity less than that of the free air) potentially fascinating for the reduction of the thermal losses of the envelopes, including those of the buildings. Thus, they can considerably contribute to the reduction of the energy consumption of this sector, which is very intensive [1, 2]. In fact, the pores of nanometric sizes allow limiting the thermal transfers via the gas phase (contained in the porosity) and thus achieve very low thermal conductivities.

In the field of the thermal insulation of buildings, nanostructured silica materials are the most studied. In addition, the pyrogenic silica and aerogel silica exhibit thermal conductivities of the order 18 $mW.m^{-1}.K^{-1}$ in normal atmospheric conditions [3, 4]. The pyrogenic silica implemented in the form of "breads" (compacted and binding) are currently being studied as the core of panels under vacuum (VIP, vacuum insulation panel) [5].

Aerogels can be either inorganic containing silica [6–11] or organic, for example, resorcinol-formaldehyde [12, 13]. They have a very low thermal conductivity, often superinsulators, and relatively fragile (aerogel of silica [14]) or made of toxic molecules (organic aerogel [15]). Mackenzie *et al*. [16] were first to develop organic-inorganic hybrid aerogel. It consists of a silica matrix consolidated by incorporation into the sol-gel of silicone macromolecules. The mechanical characteristics and thermal conductivities of the aerogels are excellent (high densities). Other hybrid aerogels were later developed [17–19]. Investigations on cellulose containing aerogels (and cellulose derivatives or other

*Corresponding authors: h.kaddami@uca.ma; yves.grohens@univ-ubs.fr
DOI: 10.7569/JRM.2017.634185

polysaccharides) were reported in many recent papers [20–23] and then a new way of research was carried out with the aim of developing superinsulating aerogel materials from bioresources. The nanocellulose used were prepared by means of TEMPO (2,2,6,6-tetramethylpiperidine-1-oxyl) oxidative pretreatment [24, 25].

On the other hand, Mobil oil company developed a new class of silicates and mesoporous aluminosilicates, so-called MCM [26, 27] and SBA-x. These materials are potential candidates for applications belonging to very varied fields such as those of catalysis, optics, sensors, processes of separation, of the adsorbents and acoustical and electrical insulation [28, 29]. The synthesis of SBA-x (x = 1, 2, 3…) and their structures (SBA: Santa Barbara) were described in 1995 in the report [30].

The combination of cellulose nanofibrils and inorganic nanoparticles yield hybrid materials with expected synergistic effects obtained when the structure of the resulting hybrid material is controlled. This synergistic effect has been widely demonstrated while studying bulk materials. For example, Liu *et al.* [31, 32] combined Montmorillonite clay and cellulose nanofibril to prepare nanopaper with high oxygen barrier properties. Other examples of synergetic properties are reported in the literature on the combination of cellulose nanofibrils and inorganic nanoparticles [33, 34].

In the present work, we propose a preparation method to obtain nanoporous hybrid aerogels based on cellulose nanofibers and silica (SBA-15) particles to achieve lower thermal conductivity of these materials. To the best of our knowledge, only a few studies [35, 36] in the literature have dealt with the application of NFC-based aerogels as a thermal superinsulator, but no studies on the combination of nanocellulose and SBA-15 to prepare and study hybrid aerogels for thermal insulation have been found.

2 MATERIALS AND METHODS

2.1 Materials

The rachis of date palm tree (*Phoenix dactylifera* L.) was used in this work as the original source of cellulose. Cellulose was extracted from the rachis following the procedure well described in our previous work [37], and the extracted cellulose will be referred to in the coming text as white paste (WP). Prior to that, the cellulose content was determined and conformed to that published in the literature [38, 39].

TEMPO, sodium bromide, sodium hypochlorite solution (15%), HCl, and NaOH were purchased from Sigma-Aldrich and used without further purification. The general procedure and reagent ratios employed by Wu *et al.* [40] were utilized for TEMPO-mediated oxidation of cellulose fibers. About 2 g, i.e., 2.136 mmol of equivalent anhydroglucose unit (AGU) of cellulose was suspended in water (200 ml) and sonicated with a Branson Sonifier for 5 min. TEMPO (32 mg, 0.065 mmol) and NaBr (0.636 g, 1.9 mmol) were added to the suspension. An additional amount of the NaOCl solution, corresponding to 40.5 ml, was versed dropwise in the cellulose suspension. The pH was adjusted at 10 by addition of a 0.1 M aqueous solution of HCl. The pH of the mixture was maintained at 10 at 4 °C by continuously adding 0.1M NaOH while stirring the suspension. After 2 hours of reaction, the oxidation was terminated by addition of methanol (5 ml) and the pH was adjusted to 7 with 0.1M HCl. In the rest of the article the NFC produced will be called NFC-2h.

After the pretreatment, a 2% fiber suspension in water was subjected to homogenizing action using a Panda 2K Laboratory Homogenizer (Gea Niro Soavi S.p.A, Italy). To obtain nanofibrillated cellulose (NFC) the oxidized cellulose was disintegrated by pumping the suspension up to 15 times through the homogenizer. Efforts were made to keep the pressure constant at 650 MPa for all cycles and all samples. During the process, the viscosity and temperature of the suspension was increased with increasing number of passes. The maximum temperature reached was 70 °C.

Silica (SiO_2) of type SBA-15 (2D-hexagonal) was provided by the Materials with Controlled Porosity team at the Institute of Materials Sciences of Mulhouse (France) under the reference C500, of morphology A (non-aggregated particles). It is formed of hexagonal particles (rods) having a diameter of about 1 µm. Silica (SBA-15) was calcined at 500 °C to eliminate the structuring and thus release the porosity. The protocol used for the synthesis of an organized mesoporous silica (OMS) of type SBA-15 was inspired by the work of Zhao *et al.* [41]. The obtained SBA-15 (2D-hexagonal) will be denoted as SBA-15 in the rest of this article.

Nanozeolites ($NaAlO_2$, SiO_2) achieved by IRMA-Ploemeur (France) under the reference A14872, were used as raw material for the preparation of the hybrid aerogels. Nanozeolites are supplied as dispersion in water. The mass concentration of the suspensions is about 20%, and the density of the zeolites is 0.3 $g.cm^{-3}$. It is formed of cubic particles having an average diameter of about 150 to 350 nm.

All chemicals utilized during this protocol had an analytical grade and were used without further purification.

2.2 Preparation of Aerogels

First of all, NFC-2h or date palm tree cellulose (WP) were resuspended separately in 50 ml of distilled water.

Silica (SBA-15) or Nanozeolites (NZs) were obtained in water solution. Then NFC-2h (NFC TEMPO treated for 2 h) or WP dispersion (depending on the targeted mixture) was passed through an Ultra-Turrax homogenizer and mixed with a specific amount of SBA-15 or NZs under magnetic stirring. The solutions were pulled in a Petri dish for one night at –20 °C and finally freeze-dried using a Christ Alpha 1–2 LDplus apparatus under 80 mBar pressure and a –52 °C temperature. Freeze-drying is carried out for 24 h to remove water traces. The elaborated aerogels were stored in an oven under vacuum at 25 °C to limit water uptake. The concentration of WP or NFC-2h was maintained constant and the SBA-15 or NZs amount varies in mass as follows: 0%, 1%, 2%, 5%, 10% and 20%. Table 1 presents the compositions of various aerogels prepared in this study.

2.3 Experimental Techniques

2.3.1 Scanning Electronic Microscope (SEM)

The SEM studies were carried out using a JEOL JSM-6460/LV microscope (Acceleration voltage: 20 kV, Working distance: ~10 mm). As the materials observed were insulating, the surfaces were metalized with an ultrathin layer of gold by sputtering with a Scancoat Six sputtering machine from Edwards. The SEM studies were carried out on a cross section of the hybrid aerogel, where the morphology is homogeneous over 100 s of µm scale.

2.3.2 Zeta Potential Measurements

Zeta potential measurements were carried out using the zeta-meter Zetasizer Nano ZS from Malvern Instruments. It is a technique of light scattering. Surface charge and the stability of the suspension of all solutions were used (WP, NFC-2h, NZs and SBA-15) and analyzed. The ionic strength of the dispersion medium was the same for all measurements.

2.3.3 Thermal Conductivity Measurements

The system utilized to measure the thermal conductivity was the "hot-filament" technique (Figure 1). The aerogel volume needed to fill the measurement chamber is 1.65 cm^3. It was composed of two cavities; one with the sample (1) and the other containing polyurethane foam (2). Both parts symmetrically surrounded a thin nickel/chrome heating filament (3). Both cavities and the filament were maintained in an isothermal box made of aluminum (4). The filament (3) was isolated from the box (4) with polymer thin films (20 µm thick) (5). The filament (3) was electrically alimented with

Table 1 Geometrical and physical characteristics of the used materials obtained at 25 °C.

Sample	Chemical structure	Pore size (nm)	Length mean ± SD (nm)	Width mean ± SD (nm)	Aspect ratio	Zeta potential (mV) (pH 5–6)	Crystalline index
Pristine Cellulose WP	Cellulose	–	$(500 \pm 30).10^3$	$(25 \pm 6).10^3$	20 ± 5	–28.3 ± 2.1	72%
Nanofibrilated Cellulose oxidized 2 h NFC	Cellulose	–	300 ± 20	20 ± 4	15 ± 5	–63.9 ± 4.3	58%
Nanozeolite (Slurry solution)	Alumino Silicate	< 2	150–350		–	–34.4 ± 0.9	> 95%
SBA-15 (2D-hex)	Silica	7	micrometric size (~1 µm)		–	–1,3 ± 0,7	–

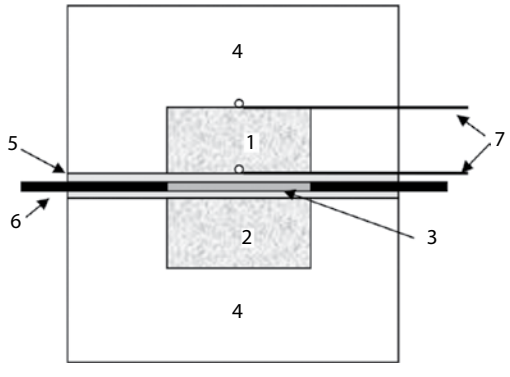

1: Aerogel to be characterized

2: Polyurethane foam

3: NiCr filament, 2µm x 4mm x 20 mm

4: Isothermal box (aluminum)

5: Thermic insulator (polymer)

6: Metallic electrodes

7: Thermocouples, type K, diameter 0.1mm

Figure 1 Scheme of the thermal conductivity measurement system.

two metallic electrodes (6). The temperature of both sides of the sample (2) was measured with two type K thermocouples (7) implemented in the system. The box (4) was thermostated at 20.7 °C with water circuit.

The thermal conductivity of the sample (1) was determined in steady state from the measurement of the conductance ribbon-housing ($W.K^{-1}$). The conductance is evaluated by the ratio of the heating measured in the center of the sample and the electric power dissipated by the sample. In our protocol, the heating is imposed and maintained at 10 °C.

The conductance is related to the sample thermal conductivity and follows a linear law depending on the measurement system: $K = A.\lambda + B$, with K ($W.K^{-1}$) being the conductance, λ ($W.m^{-1}.K^{-1}$) the thermal conductivity and A and B experimental constants depending on the sample geometry, the cavities and the thermocouples. Therefore, the first step of a measurement was the calibration of the system done by measuring the conductance of materials having a known conductivity.

2.3.4 Mechanical Properties

The mechanical properties of the hybrid aerogel were determined with dynamic mechanical analysis (DMA) realized with a DMA 2980 from TA Instruments. The compression modulus was measured on samples having the following dimensions: 25 × 25 × 4 mm^3. The tests were carried out in a controlled environment room having an ambient temperature of 23.4 °C and a humidity of 50%. The mechanical properties were determined for a frequency of 1 Hz and displacement of 0.05 mm. This technique has been used to characterize the compression modulus (E) and the yield stress (σ_y) of all hybrid aerogels.

2.3.5 Thermal Properties

Two techniques have been used to characterize the thermal properties of the materials. First, thermogravimetric analysis (TGA) was utilized to determine the loss of mass while increasing temperature. Differential thermal analysis (DTA) measured the exchange of heat during a temperature cycle. The ATG and ATD were always coupled in order to carry out the two analyses on the same sample. These analyses were conducted using a Mettler Toledo TGA/DSC thermogravimetric analyzer with 1STARe software. Approximately 50 mg of the sample was deposited in a crucible in alumina with a volume of 900 µl. Analyses were carried out under inert atmosphere (under nitrogen). The sample undergoes a rise in temperature of 20 to 600 °C with a flow of heating of 10 °C/min. The loss of weight caused by thermal degradation was recorded for each sample (against the initial weight) to identify the components degraded.

2.3.6 BET Analysis

Nitrogen adsorption/desorption isotherms were obtained using a Micromeritics ASAP 2420. The samples in the form of hybrid aerogel were placed in the measuring cell to degas all water molecules adsorbed. The degassing of the material was carried out according to the following procedure: by heating at 50 °C for 1 h and then at 100 °C for 15 h under 10^{-2} Torr. We chose relatively mild degassing conditions in order not to degrade the sample and to be sure to remove all water molecules.

Subsequently, the measuring cell was placed into an insulated tank filled with liquid nitrogen. This allows maintaining the sample at –196 °C throughout the measurement, the temperature at which gaseous nitrogen adsorption was possible on a solid surface. A nitrogen adsorption/desorption isotherm represents the evolution of the volume of nitrogen adsorbed per gram of sample extrapolated to standard conditions of temperature and pressure (STP cm^3/g) depending on the relative pressure of nitrogen ($p/p°$). Using the BET theory, it is possible to evaluate the specific surface and obtain information on the hybrid aerogel structure such as the pore size.

2.4 Physicochemical and Structural Characterization of Raw Material Solutions

In this section we report on some characteristics and physicochemical properties of the raw materials used in this study. These properties, which were obtained from previous reports we have published, are important to discuss the results on the composites' aerogel properties and structures we are presenting in the present article. Table 1 compiles all these properties.

In fact, the morphology of NFC-2h and pristine cellulose white paste (WP) was characterized by different analyses techniques (atomic force microscopy and FE-SEM) in our article [42]. The fibers in WP samples had a diameter of about 25 µm and were some hundreds of micrometers long. When oxidized for 2 hours under TEMPO treatment, fibrils obtained lower diameter (around 20 nm) and lower length (about 300 nm). This drastic reduction of the fibril diameter is the result of the homogenization step made by mechanical treatment and enhanced by oxidation process.

On the other hand, the zeta potential was measured and presented in our previous papers [24, 43]. The WP solution has a negative zeta potential of –28 ± 2 mV, which is expected for cellulose and close to the values

obtained in the literature. After 2 hours oxidation, the zeta potential decreased to –64 ± 4 mV. This is in good agreement with the fact that the oxidation process produces negative surface charges.

Moreover, the crystalline index was determined by X-ray diffraction. The pristine cellulose WP has a crystallinity of 72%. This is close to the value obtained by Benhamou *et al.* [24]. After oxidation, the crystalline index decreases to 58% [44]. The oxidation and the mechanical homogenization destroys inter- and intramolecular interactions of the cellulosic fiber. This destruction might cause the reduction of the particle crystallinity.

The silica particles SBA-15 (2D-hex) of micrometric size (~1 µm) have a pore size between 2 and 30 nm (as characterized by the supplier) and their zeta potential is close to –1.34 ± 0.69 mV for a pH of 6.3. Nanozeolite dispersions were characterized in terms of particle size of zeolites, zeta potential and pH in our paper previously published [45]. We also used the analysis of X-ray diffraction (XRD) to confirm the presence of crystallinity of zeolite. A pore size distribution between 150 to 350 nm was determined and confirmed by SEM cliché for nanozeolites [42, 45]. The aggregation process is restricted by a negative zeta potential (–34.43 ± 0.85 mV for a pH of 6.26) (Table 1) below –30 mV. This potential is sufficiently high to avoid particle interaction and to stabilize the particle suspension [46].

3 RESULTS AND DISCUSSION

3.1 Structural Characterization of the Aerogel Monoliths

In this section, our aim is to study the structure of the generated aerogel monoliths prepared by the freeze-drying of a mixture of (cellulosic materials) and (NZs or SBA-15).

After the release of ice by sublimation, the aerogels were without solvent and they looked relatively homogeneous in terms of surface smoothness. Repeatedly, streaks were visible on the surface of the obtained aerogel monoliths (Figure 2) due to the growth of ice crystals during the freezing step. After the first macroscopic observations, the aerogels appear to be relatively stiff. The films can be easily compressed by hand and return to the original position after a few minutes, showing a high elastic behavior. Neither loss nor deposition of volatile or fragile matter on hands when handling the obtained materials is observed (Figure 2). It is worth noticing that all aerogels show densities in the range of 22–24 kg.m^{-3}, which makes the comparison of their properties meaningful.

The dispersion of mineral fillers in the various celluloses has been the subject of many studies [47]. A better dispersion of the reinforcement would significantly improve the mechanical properties of materials. The quality of the dispersion and distribution of mineral charges in the various celluloses (WP and NFC-2h) were assessed through observation by SEM.

Figure 2 Photograph of aerogels dried by freeze-drying.

Figure 3 shows the SEM micrographs of the binary systems studied in this article. The cross section of aerogels obtained from pristine cellulose WP fibers of date palm tree and those mixed with 5 wt% and 10 wt% SBA-15 are depicted in Figure 3a,b and c respectively. All images are given in the same scale to facilitate the observation of the effect of dispersion based on different concentrations of SBA-15 on the pristine cellulose WP fiber surface.

Figure 3a shows the morphology for pristine cellulose WP aerogel (reference). One can estimate an average diameter of about 25 µm for individual fibers. In magnification 200x corresponding to WP (Figure 3a), it is possible to observe thin cellulose films connecting two fibers (white arrows in Figure 3a,b,c). These films result from the process and are due to the peeling of fibers during grinding and bleaching processes. We have to recall here that the structure of the WP fibers is similar to that of the cell wall fibers of wood, which consists of a multilayer structure. The SEM micrograph for the aerogels made of WP and 5 wt% SBA-15 is presented in Figure 3b. It is clearly shown in the figure that a similar structure is obtained with this mixture (WP fibers network with remaining peeled films from the process [white arrows in Figure 3b,c]). However, while zooming in on individual fibers, it's possible to observe that SBA-15 is grafted onto the WP fibers surface. Figure 3b,c highlights a good dispersion of the SBA-15 on pristine fiber surface with the presence of a few aggregates. However, beyond the 5% in weight of SBA-15 (Figure 3c), we have noticed the presence of more aggregates. In this structure, the SBA-15 is fixed to the WP fibers surface by the hydrogen bonds. On the surface of the amorphous silica walls, silanol groups have been characterized, which makes possible the

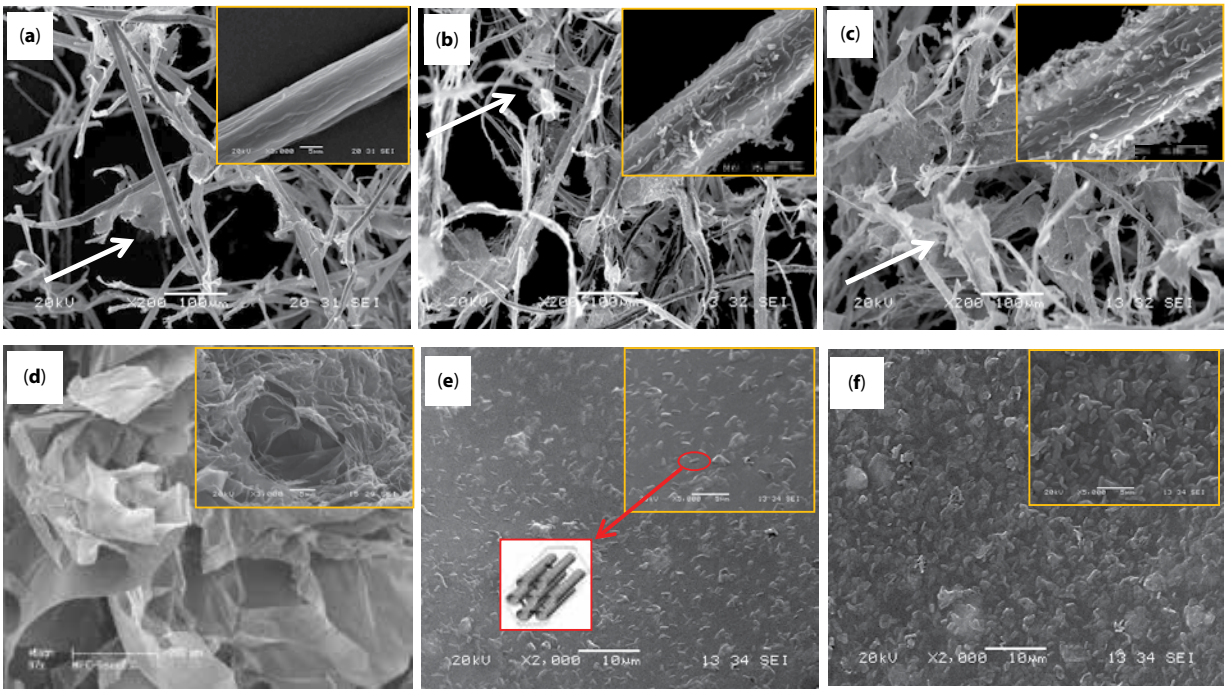

Figure 3 SEM micrographs of (**a**) Raw pristine cellulose WP, (**b**) and (**c**) are loaded respectively with 5 wt% and 10 wt% of SBA-15, (**d**) represents raw NFC-2h, (**e**) and (**f**) show NFC-2h mixed respectively with 5 wt% and 10 wt% SBA-15. White arrows show the NFC films coming from residual NFC left after purification.

formation of hydrogen bonds. On the other hand, it's well known that carboxylate groups provide emulsifying properties to the molecules or polymers that carry them. This property helps by offering good dispersion of inorganic particles in general.

Figure 3d,e,f shows the SEM micrographs of aerogel cross section made of NFC obtained after 2 hours oxidation of date palm tree fibers (NFC), SBA-15 (5 wt% and 10 wt%), respectively. For a bettter understanding, a single scale of observation has been used to highlight the dispersion effect of the SBA-15 concentration in NFC. These figures show that instead of having individual fibers, the NFCs are organized in films. This is classical for aerogels made from NFC hydrogels having a concentration higher than 0.5 wt%. The chemical groups carried by the NFC surface due to the oxidation of NFC allow forming H-bonding. This bonding allows the cellulose nanofibers to interact and to form such a uniform structure. These films can have a large area (more than 5000 µm^2 [insert in Figure 3d]). The NFC sheets are interacting together, forming a 3D network with cavities. As depicted in the micrographs, a good dispersion of SBA-15 on the NFC/SBA-15 film surface, especially at 5 wt% SBA-15, was obtained. We have noticed the presence of more and larger aggregates at concentration of 10 wt% of SBA-5 (Figure 3f). Interestingly, it seems that the concentrations of the SBA-5 particles on the NFC-2h films are higher than on the WP fibers at the same concentration of SBA-15. This may come from the zeta potential of the cellulosic fibers, which is related to the concentration of carboxylate groups on their surface. The potential of the WP (≈ –28 mV) is higher than the potential of NFC (≈ –64 mV). It means that the surface charge density is higher for NFC than WP (NFC surface contains many more carboxylate groups than WP). Therefore, the electrostatic interactions between SBA-15 and NFC are greater and a better adsorption of the SBA-15 into NFC is observed when compared to WP.

We can draw a few conclusions based on this study. The adsorption of SBA-15 is easier on NFC compared to WP. The aggregation of SBA-15 particles is observed only when their concentration exceeds 5 wt%. The morphology of both systems is different: individual fibers of WP and films of NFC. These differences in morphology might be driven by the charge of the particles, their aspect ratio and concentrations. We also discussed how the properties of each constituent influences the structure of the hybrid aerogels. Now, the study will focus on the influence of the specific structures on the thermal and mechanical properties.

3.2 Thermal Characterization of Aerogels

We are interested in having tunable thermal properties from designed hybrid materials.

3.2.1 Effect of SBA-15 on the Thermal Conductivity of WP and NFC-2h-Based Aerogels

Prior to discussing the effect of SBA-15 on the thermal conductivity of the studied cellulosic aerogels, it is worth having a global discussion on the thermal conductivity of the two families of materials (WP-based materials and NFC-based materials) based on their morphologies. In fact, the thermal conductivity is the combination of several contributions [48, 49]. The measured thermal conductivity is the sum of the convective thermal conductivity (negligible in the case of mesopores, but higher with macropores), the radiative thermal conductivity (that depends on the opacity of the material), the solid thermal conductivity (coming from the density of the material and the thermal conduction through the solid skeleton) and the gaseous thermal conductivity (related to the pore size via Knudsen effect and the collision of gas molecules). Figure 4 depicts the evolution of thermal properties of aerogels formed from cellulosic mixtures of WP or NFC with the various concentrations of SBA-15 (density ~22 $kg.m^{-3}$). From this figure, it is interesting to notice that globally the aerogels based on cellulosic microfiber (WP) show higher thermal conductivity compared to the aerogel based on nanofibrillated cellulose (NFC). From a morphological point of view, this behavior was predictable since the morphologies and the sizes of the porous structures are different. This also is in agreement with the results we have published recently [42, 44]. In fact, Figure 3a,d highlights two very different organizations. From WP, the cellulose fibers generate a 3D network having macropores (roughly between 200 to 300 µm determined by SEM image analysis). The pores are formed by the space between fibers. For NFC, the structure obtained is films stacked on top of each other, which form cavities having a smaller size than that observed between the WP fibers. The high thermal conductivity obtained for the WP-based aerogel probably arises from the fact that convective processes are possible in the macropores. There is also a huge gas conduction contribution as the air molecules can interact with pore sizes higher than their mean free distance. However, in the case of NFC-based aerogel, the lower size of the pore reduces the convective contribution. Therefore, the thermal conductivity is relatively lower than that of the WP-based aerogels. It's also possible that some mesopores would be present in the structure. It was reported that the films forming the cavities in NFC-based aerogel should contain pores of nanometric sizes [50]. This would further lower the gas conduction contribution and contribute to the decrease in the effective thermal conductivity.

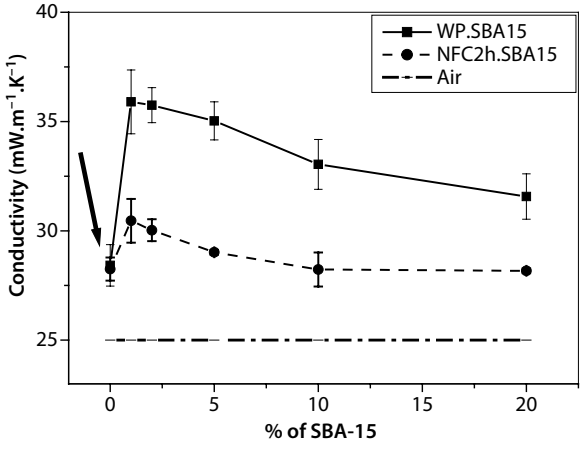

Figure 4 Influence of the SBA-15 concentration of various solutions on the thermal properties of the WP and NFC aerogels. Arrow indicates similar thermal conductivity of WP and NFC without SBA-15.

At a temperature equal to 22 °C and for a density close to 176 $kg.m^{-3}$, the thermal conductivity of silica SBA-15 is equal to 32.51 $mW.m^{-1}.K^{-1}$, close to that of zeolites (31.68 $mW.m^{-1}.K^{-1}$) and nanozeolites (31.64 $mW.m^{-1}.K^{-1}$). This slight difference in the conductivity is due to the morphology and pore size of particles (presence in silica SBA-15 of pores larger than 2 to 30 nm and superior to zeolites) [51]. In Figure 4, plain and dashed lines show the evolution of the thermal conductivity of aerogels based on WP/SBA-15 and NFC/SBA-15. The fraction of nanoparticles has been varied from 1 to 20 wt%. Interestingly, the thermal conductivity of the hybrid aerogel based on cellulose WP with a 1 wt% concentration of SBA-15 increased compared to neat cellulose WP aerogels. However, for the aerogels with contents of SBA-15 of 2 wt% or more, a decrease of the effective thermal conductivity is observed when silica SBA-15 content increases. The same trend is observed for NFC-2h/SBA-15 aerogels: an increase followed by a decrease appeared when adding silica SBA-15 to the hybrid aerogel. However, we found that their thermal conductivities are inferior to that of WP/SBA-15 aerogels. From these results, we can conclude that the larger the cellulosic fiber is, the higher the thermal conductivity. This comes from the arrangement discussed above, which is governed by the interactions and the charge of the used cellulosic particles.

Moreover, the decrease of the thermal conductivity observed in the systems based on cellulose WP is because of the presence of silica SBA-15 particles, which have internal pores in their structure (presence of mesoporosity) which decrease the gas conduction contribution (Figure 5a). However, the decrease of the thermal conductivity for the NFC-2h-based aerogels is due to both the internal porosity of silica SBA-15 (mesoporosity), to the tighter entanglement of the fibers

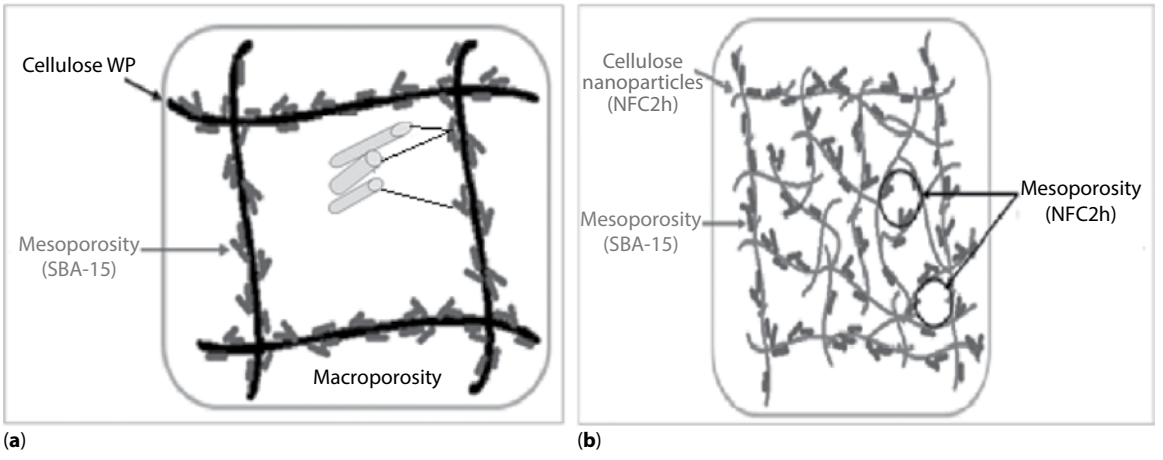

Figure 5 Theoretical diagram of hybrid aerogel based on: (**a**) Pristine long fibers WP (black) with macroporosity and SBA-15 (blue); and (**b**) Cellulose nanoparticles NFC-2h (red) and SBA-15 (blue) with mesoporosity.

and the smaller size of nanofibers NFC-2h (Figure 5b). The latter create pores of smaller size than the mean free path of air molecules (~70 nm at atmospheric pressure and ambient temperature), which allows significant reduction of the contribution of the gas phase, by Knudsen effect, and the achievement of interesting thermal properties.

The formulation NFC-2h/SBA in the range of 15–20 wt% has a thermal conductivity much lower (28.17 $mW.m^{-1}.K^{-1}$) compared to other hybrid systems. Thus, the nanostructured network based on nanofibers NFC-2h shows the best thermal insulation properties. The values of thermal conductivity of these hybrid aerogels based on nanofibers are very interesting and are almost in the same order of magnitude of those obtained for polymeric aerogels [52]. These experiments certainly open the way for new applications of NFC-based aerogels as insulating materials. Most aerogel materials used in insulating applications show thermal conductivity higher than 20 $mW.m^{-1}.K^{-1}$ [53, 54]. The obtained values (from 28 to 32 $mW.m^{-1}.K^{-1}$) of the thermal conductivity for the hybrid aerogel-based WP/SBA-15 and NFC-2h/SBA-15 are very close to that obtained for cellulose aerogels from paper waste reported by Nguyen *et al.* [55]. The thermal conductivity of NFC-2h/SBA-15 and WP/SBA-15 hybrid aerogels is comparable to other composite aerogels reported elsewhere [56, 57] and conventional thermal insulators such as mineral wools and polymer foams.

3.2.2 Comparison Between the Effects of NZ- and SBA-15-Based Aerogels

In this section, the thermal conductivities of hybrid aerogel NFC/SBA-15 are compared to those based on

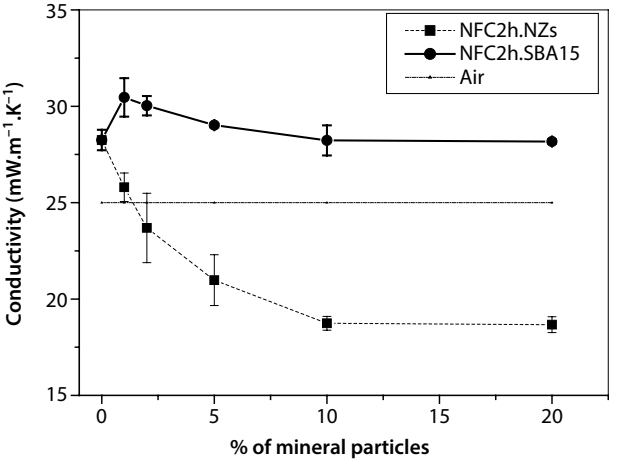

Figure 6 Influence of the NZs and SBA-15 concentration of various solutions on the thermal properties of the NFC-2h aerogels.

NFC and nanozeolites. We have determined the mineral load for the composite which gives the best insulation property. The values of the thermal conductivity of the NFC/NZ hybrid aerogels are reported from our previous studies [65].

Figure 6 depicts the evolution of thermal properties of aerogels formed from cellulosic mixtures of NFC with the various concentrations of NZs or SBA-15, whose density is known (d ~ 20 $kg.m^{-3}$). From this figure, it is interesting to notice that for the system based on NFC-2h, the thermal conductivity of the binary formulation NFC-2h/20%-NZs is equal to 18.67 $mW.m^{-1}.K^{-1}$, which is lower than that of the air (~ 25 $mW.m^{-1}.K^{-1}$). The introduction of nanozeolites induces an insulating effect much more important than the silica particles SBA-15 with the NFC-2h. This effect is

due to the pore size of the mineral charges. Zeolites are microporous materials with pore sizes < 2 nm [58] and silica SBA-15 presents pore sizes larger than zeolites (from 2 to 30 nm). As a result, the dominant conduction for the two systems (NFC-2h/NZs and NFC-2h/SBA-15) is gaseous conduction (a strong confinement of free air between the NFC-2h films and meso- or microporosity of mineral charges), which directly controls the overall conductivity.

The thermal conductivity values (~18 to 28 $mW.m^{-1}.K^{-1}$) obtained for these hybrid aerogels are lower than those obtained by Nguyen *et al.* (32 $mW.m^{-1}.K^{-1}$) [59] for cellulose aerogels prepared from paper waste or wool (30–40 $mW.m^{-1}.K^{-1}$). However, they are comparable to those having the best thermal insulation such as the silica aerogel (26 $mW.m^{-1}.K^{-1}$), and aerogels produced by the Aspen group (21 $mW.m^{-1}.K^{-1}$) [60, 61]. This low value of thermal conductivity leads to a promising material for thermal insulation. The studied aerogels are classified as thermal superinsulators because they have less thermal conductivity than the air (~25 $mW.m^{-1}.K^{-1}$).

To verify the influence of the NFC aerogels' pore size on thermal conductivity, Nitrogen adsorption experiments were carried out. From the results obtained by this technique, the porosities of all formulations developed were determined. Also, the specific surface area has been conventionally estimated by the method of Brunauer, Emmett and Teller BET (S_{BET}) [62, 63]. The general trend for the evolution of the specific surface area is: S_{BET} of cellulose microfibers (WP)-based aerogels are higher than those estimated for NFC-based ones. For WP, the specific surface is close to 195 m^2/g when adding 20 wt% of nanozeolites, while for nanofibrillated cellulose (NFC) it is close to 100 m^2/g when adding 20 wt%, and similar results are obtained by the system based on SBA-15. However, in light of specific surface areas and mean diameters of the particles constituting the fibrillary mesoporous network (ranging from 2 to 50 nanometers), one can qualitatively conclude that the solid skeleton of hybrid aerogels is nanostructured. This effect is not intuitive. In order to explain this observation, we conjecture that the NFC films are surrounding NZs and SBA-15 particles, which reduces the accessibility of nitrogen molecules to the internal porous structure of the nanozeolites and silica particles. The low thermal conductivity values for NFC/NZs and NFC/SBA-15 are interpreted by the coexistence of the nanozeolites and silica pores, which are non-accessible to nitrogen, and interfibrillar cellulose pores that nitrogen can easily probe.

However, compared with most other aerogels (silica and resorcinol-formaldehyde aerogels), these specific surface values appeared to be relatively low. It suggests the existence of a small proportion of nanopores or poor accessibility to the latter. Macropores observed by SEM (Figure 3a) on the cross section of the aerogels dominate the hybrid aerogel structures as suggested previously. The results obtained from the specific surface area by BET for our materials are superior to those described by Silva *et al.* [64] for cellulose aerogels obtained after freeze-drying. However, they are close to those gained by Sehaqui *et al.* [65] for aerogels based on nanofibrillated cellulose prepared by 6-step solvent exchange followed by CO_2 supercritical drying.

3.3 Aerogel Mechanical Properties

Many aerogels have good insulation properties, but their mechanical properties are not good enough to make them industrially utilizable. In this section, we are interested in having tunable mechanical properties from the designed hybrid materials. Also, one of the very interesting properties of such a monolith compared to other inorganic materials is its elasticity. Therefore, it is necessary to optimize the interactions and improved mechanical properties.

3.3.1 Effect of SBA-15 on the Mechanical Properties of WP- and NFC-2h-Based Aerogels

From compression stress-strain tests the mechanical characteristics such as compression modulus E and the yield stress have been deducted according to the article published by Gibson and Ashby [66]. Figure 7 shows the evolution of the mechanical properties of hybrid aerogels based on WP and NFC-2h with silica SBA-15 used as nanofillers. The fraction of nanofillers has been varied from 1 to 20 wt%.

The stiffness measured by the compression modulus E is higher for the aerogel formed by the NFC-2h than from the WP without SBA-15. To explain this difference, one should refer to the structural differences of the two aerogels. For WP, the system is organized as a fiber network and the possible interactions are therefore due to the interaction between two micrometric fibers (cylinders). Then the contact area can be assimilated to a point. However, for the NFC-2h aerogel, in which the system formed as films where the contact area is the contact of two plans, the contact area between neighboring NFCs can be assimilated to a curve. The contact area is then higher for NFC-2h system than for WP system. This indicates that the induced cohesive forces are higher for the NFC-2h system, the network then is more difficult to compress. It has also been shown that the pore size is bigger for WP and allows more compressibility of the system before reaching the

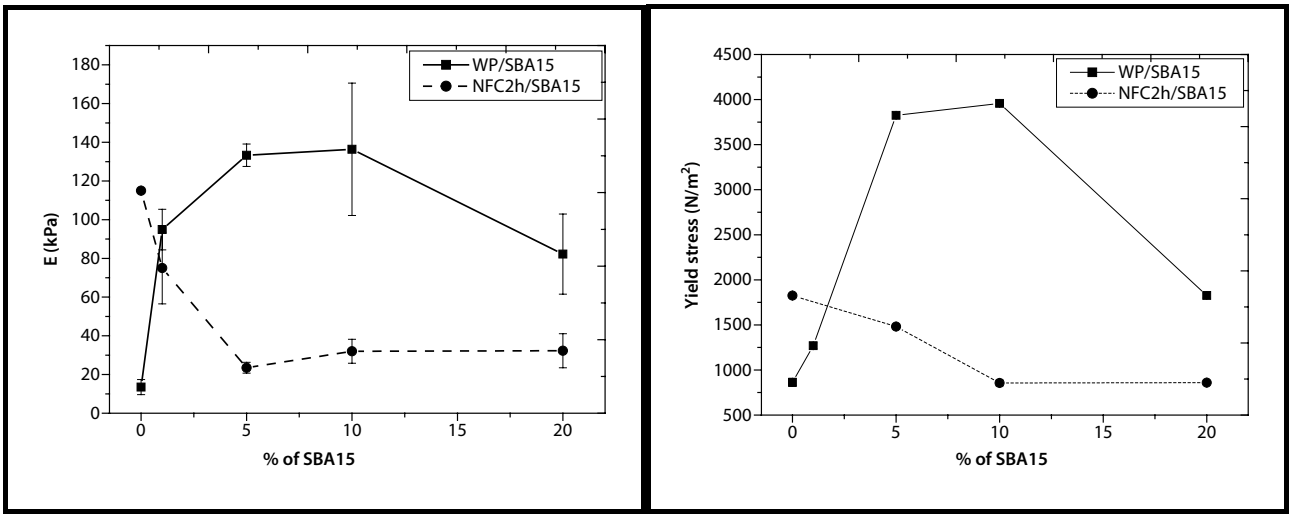

Figure 7 (**a**) Evolution of the compression modulus (E) and (**b**) the yield stress (σs) with the wt% of the silica SBA-15 added for the hybrid aerogels based on WP and NFC.

network rupture force. This is in agreement with the observations made by other groups working on nanopapers [67]. The reinforcement in these aerogels seems to be governed more by the strength of the interactions between the various components.

At the micrometric scale (WP), the silica particles (SBA-15) provide a mechanical reinforcement in the cellulose up to 10 wt% (compression modulus moves from 13.5 kPa to 136.4 kPa). These developments highlight that the mechanical performance is determined based on reinforcement provided by the silica (SBA-15) to cellulose. Good mechanical properties are also observed for the WP/SBA15–10 wt% formulations. By contrast, a negative effect on the mechanical properties has been observed by the introduction of silica (SBA-15) in the formulations based on NFC-2h. These results for the systems based on NFC-2h are unexpected, i.e., the strain increases slightly (results are not shown here) while the yield stress and the module decrease when the percentage of mineral load increases. According to the literature [68–70], when the organic polymer is filled by aggregates of mineral charges, the hardness of the aerogel, the modulus of elasticity and the stress fall significantly. Therefore, aggregations of silica particles SBA-15 and their micrometric size have a negative and strong influence, especially on the mechanical properties for the binary system based on NFC-2h. This loss of mechanical properties of the hybrid aerogels is not prohibitive for the commercial use of the aerogels as insulators. However, it is worth noticing that these hybrid aerogels show similar elastic behavior against compression as the PMSQ-CNF composite aerogels [52]. The values of the compression module for the hybrid aerogels (13–136 kPa) are higher than those obtained by Nguyen *et al.* (11 kPa) [71].

3.3.2 Comparison Between the Effects of NZ- and SBA-15 Based Aerogels

In order to compare the effect of loading and nature of the mineral load on mechanical properties, hybrid aerogels are represented in Figure 8. The results reported for the nanozeolite (NZ)-based hybrid aerogels are reported from our previous studies [42].

For the hybrid aerogels based on cellulose WP, the addition of the mineral charges, NZs or silica SBA-15, led to a significant increase in the modulus. These evolutions highlight the phenomenon of mechanical reinforcement provided by these mineral charges to the cellulose WP. As a comparison, we have noticed that the silica particles have an effect of reinforcement much larger than nanozeolites in the case of aerogel based on cellulose WP, especially beyond 4 wt% of the mineral filler. Moreover, above this weight fraction, although higher than unfilled aerogel, the modulus decreases strongly for the aerogel-based WP/NZs in comparison to the WP/SBA-15-based ones.

However, in the case of NFC-based aerogel the variations of the modulus observed with the increase of the nanozeolites' load have very little significance (or even negligible). Furthermore, the modulus decreases strongly by the addition of silica (SBA-15) in the material. In this latter case, this evolution may be due to the clustering of SBA-15 silica particles in the form of aggregates in the hybrid aerogels. In the case of NFC-based aerogels the agregates are significantly smaller

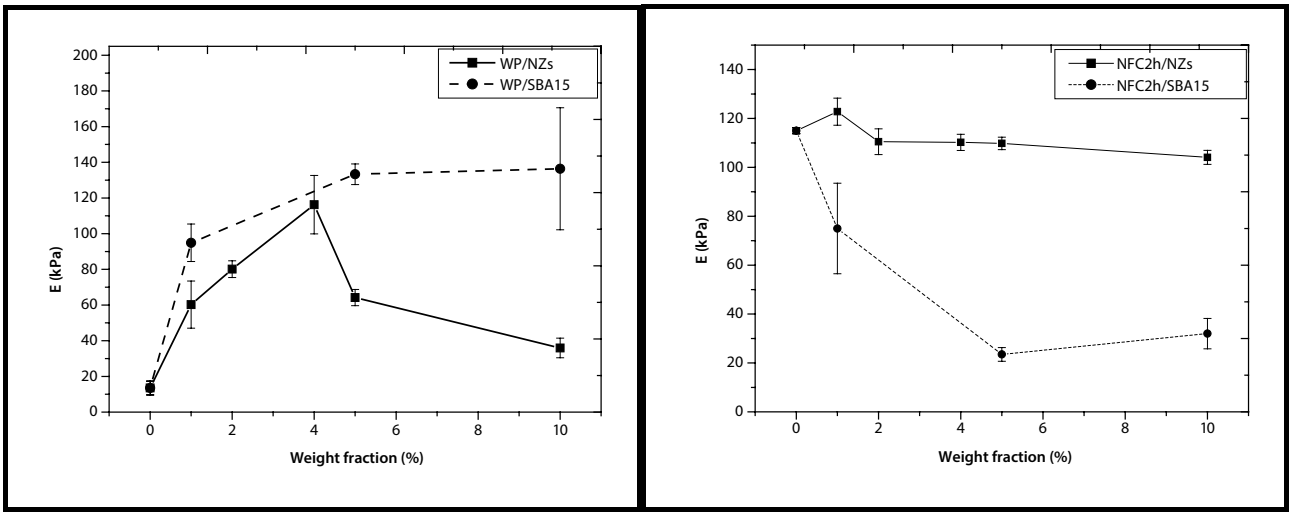

Figure 8 Influence of the NZs and SBA-15 concentration of various solutions on the compression modulus of the (**a**) WP and (**b**) NFC-2h hybrid aerogels.

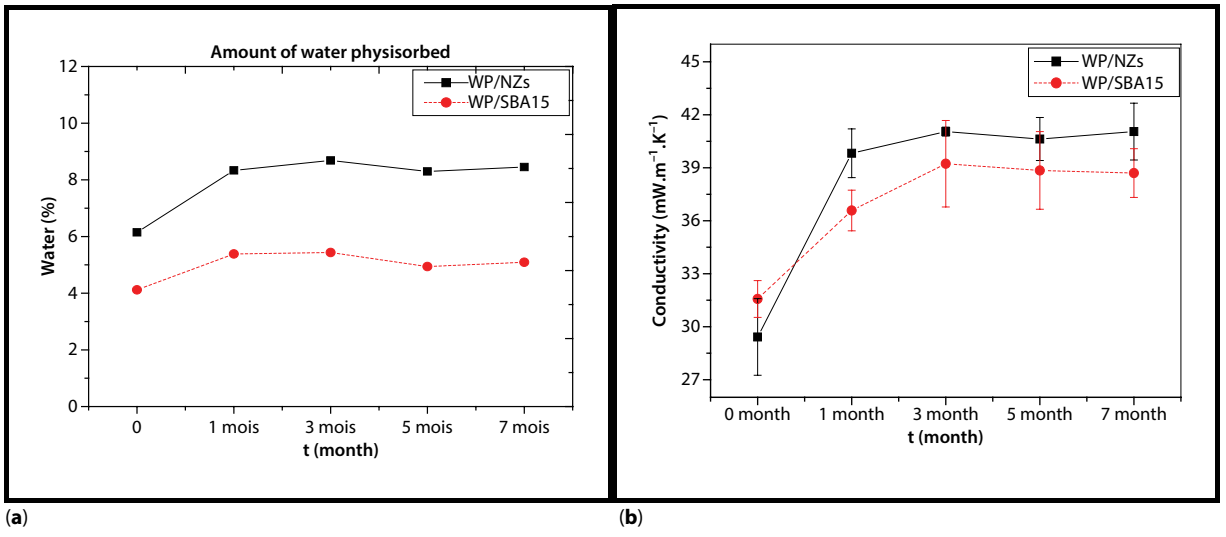

Figure 9 Evolution of (**a**) % of the sample mass corresponding to the physisorbed water determined by TGA as a function of time, and (**b**) of the thermal conductivity as a function of time in a free atmosphere (50% HR and 23 °C).

[42], which could explain ther negligible effect on the modulus.

3.4 Influence of Moisture on the Thermal Conductivity of the Hybrid Aerogel in a Free Atmosphere

This section of the study was performed on the hybrid aerogel based on WP fibers filled with 20 wt% of inorganic filler (NZs and SBA-15). The TGA experiment of the hybrid aerogel shows two mass-loss events corresponding to two endothermic peaks for the lost of physisorbed water (T < 100 °C) and for the decomposition of the organic matter (especially cellulose) under inert atmosphere in higher tempeatures.

From these analyses, performed on WP/NZs and WP/SBA-15, we were able to construct the curve of evolution of the amount of water absorbed over time (Figure 9a). We have observed that the hybrid aerogels absorb the water especially during the first months. Indeed, during the first month, these materials exhibit a sharp increase in the percentage of adsorbed water to achieve a quantity of 2 wt%. The water continues to adsorb on the surface of the material up to 3 months,

when we observed that the system was saturated after adsorption of a fraction of 3 wt%. Therefore, the water saturation of the hybrid aerogel in a free atmosphere varies from 8 to 12 weeks. However, even the initial amounts of the adsorbed water for both aerogels were different; the same amount of water has been adsorbed after conditioning at 50% RH and 23 °C. The higher amount of adsorbed water by WP/NZs composite before conditioning could be explained by the low size of the NZs that confers on them a higher surface and then higher contact surface with water molecules.

In parallel to the measurements of water absorption, the thermal conductivity has been measured and the results are shown in the graph in Figure 9b.

After one month, the amount of sorbed water for WP/NZs-20 hybrid aerogels increased from 6 wt% to 8 wt%, which has a significant impact on its thermal conductivity, which increased from 29.4 $mW.m^{-1}.K^{-1}$ to 39.8 $mW.m^{-1}.K^{-1}$. Similar results are observed for the WP/20%SBA-15 hybrid aerogel for which the thermal conductivity increased from 31.6 $mW.m^{-1}.K^{-1}$ to 36.6 $mW.m^{-1}.K^{-1}$ after having adsorbed an additional 1.4 wt% of water. Beyond one month of exposure to 50% HR at 23 °C, no significant increase of the adsorbed water has been registered for the two aerogels and their thermal conductivities remain stable. Therefore, the performance of the insulating materials is clearly degraded by moisture.

The influence of moisture on the thermal transfers differs depending on the state of the water present in the matrix of the material gaseous state (water vapor) or condensed state (water adsorbed on the surface of the material). Many teams [72–75] have studied the impact of moisture content on the thermal conductivity of the insulating materials, more particularly with materials that have a hydrophilic character such as precipitated silica and pyrogenic silica. These researchers measured the thermal conductivity as a function of the water quantity present in the material using the hot-plate method [72, 73]. According to their results, it appears that the thermal conductivity increases linearly with the increase of the quantity of water present in the matrix of the silicic material. This enables them to determine a proportionality coefficient "B" according to the Equation 2:

$$\frac{\partial \lambda_{tot}}{\partial u} = B \quad (2)$$

where "λ_{tot}" is the thermal conductivity and "u" is the amount of water in the materiels.

The coefficient B represents in a comprehensive manner the degree of influence of the water content (water vapor + condensed water) on the thermal conductivity. The larger this proportionality factor is, the greater is the impact of water present in the material on the thermal conductivity. This also reflects the strong hydrophilic character of the material. Quénard *et al.* [76] have calculated a value of 1.4 $mW.m^{-1}.K^{-1}.\%$ for this proportionality factor for a pyrogenic silica sample of a density of 162 $kg.m^{-3}$ at 296 K under atmospheric pressure.

The linearity between the thermal conductivity and the mass quantity of water is always maintained even under a high vacuum. Heinemann [77] has confirmed this linearity between the thermal conductivity and the mass quantity of water in the material. He has calculated the proportionality coefficient for a pyrogenic silica sample of a density of 170 $kg.m^{-3}$ at a temperature of 293 K, and the coefficient is much lower than under atmospheric pressure, 0.3 $mW.m^{-1}.K^{-1}.\%$.

In our case, we measured the thermal conductivity using the hot-ribbon method and as a function of the quantity of water present in the material. According to the results, we have noticed that the thermal conductivity increases linearly with the increase of the quantity of water present in the mineral charges (NZs and SBA-15). The proportionality coefficient under atmospheric pressure for the hybrid aerogel based on WP/20 wt% SBA-15 is around 7.4 $mW.m^{-1}.K^{-1}.\%$ and hybrid aerogel based on WP/20 wt% NZs has a value of coefficient much lower, about 4.8 $mW.m^{-1}.K^{-1}.\%$, at 296 K. This significant variation of the thermal conductivity reflects the degradation of the thermal insulation performance that may occur in these materials in contact with moisture (free atmosphere of 50% HR and 23 °C).

4 CONCLUSION

The structures of designed hybrid aerogels were governed by the aspect ratio of the suspended particles, their charge via electrostatic forces, zeta potential and hydrogen bond. We observed two particular organizations for WP fibers and NFC-2h, which are individual fibers and thin films, respectively. The properties of the used mineral particles (NZs or SBA-15) greatly influence the aerogel thermal behavior through morphological changes. The resulting NFC films embed mineral charges porous structure and yield a decrease in the specific surface measured by BET. Enclosing the mineral particle pores into the mesoporous network is beneficial to the thermal insulation properties of the NFC-2h aerogels, and the mechanical properties of WP-based aerogels are positively affected by the mineral particles. Finally, we showed that the moisture negatively affects the thermal insulating properties of these aerogels.

ACKNOWLEDGMENTS

We are grateful for Anthony Magueresse's help with the SEM and FE-SEM experiments. The authors thankfully acknowledge the Center of Analyses and Characterizations (CAC) of Cadi Ayyad University (CAC-UCA)-Morocco, Bretagne region, the European Union (FEDER), and the French Ministry of Research for rendering financial support for conducting the studies.

REFERENCES

1. K.I. Jensen, Passive solar component based on evacuated monolithic silica aerogel. *J. Non Cryst. Solids* **145**, 237 (1992).
2. T. Woignier, G.W. Scherer, and A. Alaoui, Stress in aerogel during depressurization of autoclave: II. Silica gels. *J. Sol-Gel Sci. Technol.* **3**, 141 (1994).
3. C.J. Brinker, and G.W Scherer, *Sol-Gel Science*, Academic Press Inc.: London (1990).
4. S. Hæreid, J.M. Anderson, M.A. Einarsrud, D.W. Hua, and D.M. Smith, Thermal and temporal aging of TMOS-based aerogel precursors in water. *J. Non Cryst. Solids* 185, 221 (1995).
5. R.W. Pekala, *et al*., Carbon aerogels, in: *Sol-Gel: Processing and Applications*, p. 369, Plenum: New York (1994).
6. D.M. Smith, W.C. Ackerman, and A. Maskara, Compositions and insulation bodies having low thermal conductivities, US Patent 5877100, assigned to Cabot Corporation (1999).
7. A. Bisson, A. Rigacci, P. Achard, M.D. Candido, P. Florent, G. Pouleyrn, and P. Bonnardel, Preparation of silicaxerogels, FR 2873677, assigned to Armines (2006).
8. C. Langlais, and S. Klarsfeld, Isolation thermique à température ambiante. Bases physiques. *Techniques de l'Ingénieur* BE 9860 (1997).
9. J. Fricke, E. Hümmer, H.J. Morper, and P. Scheuerpflug, Thermal properties of silica aerogels. *J. Phys. Colloq.* **50**(C4), 87–97 (1989).
10. J. Phalippou, T. Woignier, and M. Prassas, Glasses from aerogels, Part I: The synthesis of monolithic aerogels. *J. Mater. Sci.* **25**, 3111 (1990).
11. N. Hüsing, and U. Schubert, Aerogels-airy materials: Chemistry, structure, and properties. *Angew. Chem. Int. Ed.* **37**, 22 (1998).
12. R.W. Pekala, Organic aerogels from polycondensation of resorcinol with formaldehyde. *J. Mater. Sci.* **24**, 3221–3227 (1989).
13. R.W. Pekala, Low density resorcinol-formaldehyde aerogels, US Patent 4873218, assigned to U.S. Department of Energy (1989).
14. R.W. Pekala, C.T. Alviso, and J.D. Le May, Organic aerogels: Microstructural dependence of mechanical properties in compression. *J. Non Cryst. Solids* **125**, 67–75 (1990).
15. X. Lu, R. Caps, J. Fricke, C.T. Alviso, and R.W. Pekala, Correlation between structure and thermal conductivity of organic aerogels. *J. Non Cryst. Solids* **188**, 226–234 (1995).
16. J.D. Mackenzie, et al., Rubber ormosils and their applications. *J. Non Cryst. Solids* **147**, 148–271 (1992).
17. G.M. Pajonk, Aerogel synthesis, in: *Catalyst Preparation: Science and Engineering*, J. Regalbuto (Ed.), pp. 31–45, CRC Press Taylor & Francis Group (2006).
18. Aspen Aerogels, Spaceloft 6250 (retrieved April 25, 2014).
19. Aerogel.org, Strong and Flexible Aerogels (retrieved July 17, 2014).
20. F. Fischer, A. Rigacci, R. Pirard, S. Berthon-Fabry, and P. Achard, Cellulose-based aerogels. *Polymer* **47**, 7636–7645 (2006).
21. C.A. García-González, M. Alnaief, and I. Smirnova, Polysaccharide-based aerogels: Promising biodegradable carriers for drug delivery systems. *Carbohydr. Polym.* **86**, 1425–1438 (2011).
22. E. Guilminot, R. Gavillon, M. Chatenet, S. Berthon-Fabry, A. Rigacci, and T. Budtova, New nanostructured carbons based on porous cellulose: Elaboration, pyrolysis and use as platinum nanoparticles substrate for oxygen reduction electrocatalysis. *J. Power Sources* **185**, 717–726 (2008).
23. R. Sescousse, R. Gavillon, and T. Budtova, Aerocellulose from cellulose-ionic liquid solutions: Preparation, properties and comparison with cellulose-NaOH and cellulose-NMMO routes. *Carbohydr. Polym.* **83**, 1766–1774 (2011).
24. K. Benhamou, A. Dufresne, A. Magnin, G. Mortha, H. Kaddami, Control of size and viscoelastic properties of nanofibrillated cellulose from palm tree by varying the TEMPO-mediated oxidation time. *Carbohydr. Polym.* **99**, 74–83 (2014).
25. Y. Okita, T. Saito, and A. Isogai, Entire surface oxidation of various cellulose microfibrils by TEMPO-mediated oxidation. *Biomacromolecules* **11**, 1696–1700 (2010).
26. C.T. Kresge, M.E. Leonowicz, W.J. Roth, J.C. Vartuli, and J.S. Beck, Ordered mesoporous molecular sieves synthesized by a liquid-crystal template mechanism. *Nature* **359**, 710 (1992).
27. J.S. Beck, J.C. Vartuli, J. Roth, M.E. Leonowicz, C.T. Kresge, K.D. Schmitt, C.T.W. Chu, D.H. Olson, E.W. Sheppard, S.B. McCullen, J.B. Higgins, and J.L. Schlenker, A new family of mesoporous molecular sieves prepared with liquid crystal templates. *J. Am. Chem. Soc.* **114**, 10834 (1992).
28. A. Imhof, and D.J. Pine, Ordered macroporous materials by emulsion templating. *Nature* **389**, 948 (1997).
29. J.E.G. Wijnhoven, and W.L. Vos, Preparation of photonic crystals made of air spheres in titania. *Science* **281**, 802 (1998).
30. Q. Huo, R. Leon, P.M. Petroff, and G.D. Stucky, Mesostructure design with gemini surfactants: Supercage formation in a three-dimensional hexagonal array. *Science* **268**,1324 (1995).
31. A. Liu, A. Walther, O. Ikkala, L. Belova, and L.A. Berglund, Clay nanopaper with tough cellulose nanofiber matrix for fire retardancy and gas barrier functions. *Biomacromolecules* **12**, 633–641 (2011).

32. A. Liu, and L.A. Berglund, Fire-retardant and ductile clay nanopaper biocomposites based on montmorrilonite in matrix of cellulose nanofibers and carboxymethyl cellulose. *Eur. Polym. J.* **49**, 940–949 (2013).
33. D.O. Carlsson, G. Nyström, Q. Zhou, L.A. Berglund, L. Nyholm, and M. Strømme, Electroactive nanofibrillated cellulose aerogel composites with tunable structural and electrochemical properties. *J. Mater. Chem.* **22**, 19–14 (2012).
34. H. Koga, A. Azetsu, E. Tokunaga, T. Saito, A. Isogai, and T. Kitaoka, Topological loading of Cu(I) catalysts onto crystalline cellulose nanofibrils for the Huisgen click reaction. *J. Mater. Chem.* **22**, 5538 (2012).
35. T.C.F. Silva, Y. Habibi, J.L. Colodette, T. Elder, and L.A. Lucia, A fundamental investigation of the microarchitecture and mechanical properties of tempo-oxidized nanofibrillated cellulose (NFC)-based aerogels. *Cellulose* **19**, 1945–1956 (2012).
36. Z. Yuan, Q. Fan, X. Dai, C. Zhao, A. Lv, J. Zhang, G. Xu, and M. Qin, Cross-linkage effect of cellulose/laponite hybrids in aqueous dispersions and solid films. *Carbohydr. Polym.* **102**, 431–437 (2014).
37. H. Jin, A. Cao, E. Shi, J. Seitsonen, L. Zhang, R.H.A. Ras, L.A. Berglund, M. Ankerfors, A. Walther, and O. Ikkala, Ionically interacting nanoclay and nanofibrillated cellulose lead to tough bulk nanocomposites in compression by forced self-assembly. *J. Mater. Chem. B* **1**, 835–840 (2013).
38. A. Bendahou, T. Habibi, A. Dufresne, and H. Kaddami, Physico-chemical characterization of palm from *Phoenix dactylfera*-L, preparation of cellulose whiskers and natural rubber-based nanocomposites. *J. Biobased Mater. Bioenergy* **3**(1), 81–90 (2009).
39. M. Jouiad, N. Al-Nofeli, N. Khalifa, F. Benyettou, and L.F. Yousef, Characteristics of slow pyrolysis biochars produced from rhodes grass and fronds of edible date palm. *J. Anal. Appl. Pyrolysis* **111**, 183–190 (2015).
40. C.N. Wu, T. Saito, S. Fujisawa, H. Fukuzumi, and A. Isogai, Ultrastrong and high gas-barrier nanocellulose/clay-layered composites. *Biomacromolecules* **13**, 1927–1932 (2012).
41. D. Zhao, J. Feng, Q. Huo, N. Melosh, G.H. Fredrickson, B.F. Chmelka, and G.D. Stucky, Triblock copolymer syntheses of mesoporous silica with periodic 50 to 300 angstrom pores. *Science* **279**(5350), 548–552 (1998).
42. D. Bendahou, A. Bendahou, B. Seantier, Y. Grohens, and H. Kaddami, Nano fibrillated cellulose-zeolites based new hybrid composites aerogels with super thermal insulating properties. *Ind. Crops Prod.* **65**, 374–382 (2015).
43. A. Kadimi, K. Benhamou, Z. Ounaies, A. Magnin, A. Dufresne, H. Kaddami, and M. Raihane, Electric field alignment of nanofibrillated cellulose (NFC) in silicone oil: Impact on electrical properties. *ACS Appl. Mater. Interfaces* **6**(12), 9418–9425 (2014).
44. D. Bendahou, A. Bendahou, B. Seantier, Y. Grohens, and H. Kaddami, Multi-scale cellulose based new bio-aerogels composites with thermal super-insulating and tunable mechanical properties. *Carbohydr. Polym.* **138**, 335–348 (2016).
45. D. Bendahou, A. Bendahou, Y. Grohens, and H. Kaddami, New nanocomposite design from zeolite and poly(lactic acid). *Ind. Crops Prod.* **72**, 107–118 (2015).
46. R. Tantra, P. Schulze, and P. Quincey, The effect of nanoparticle concentration on zeta-potential measurement results and reproducibility. *Particuology* **8**, 279–285 (2010).
47. Z. Yuan, Q. Fan, X. Dai, C. Zhao, A. Lv, J. Zhang, G. Xu, and M. Qin, Cross-linkage effect of cellulose/laponite hybrids in aqueous dispersions and solid films. *Carbohydr. Polym.* **102**, 431–437 (2014).
48. O.J. Lee, K.H. Lee, T.J. Yim, S.Y. Kim, and K.P. Yoo, Determination of mesopore size of aerogels from thermal conductivity measurements. *J. Non Cryst. Solids* **298**, 287–292 (2002).
49. X. Lu, R. Caps, J. Fricke, C.T. Alviso, and R.W. Pekala, Correlation between structure and thermal conductivity aerogels of organic. *J. Non Cryst. Solids* **188**, 226–234 (1995).
50. H. Fukuzumi, T. Saito, S. Iwamoto, Y. Kumamoto, T. Ohdaira, R. Suzuki, et al., Pore size determination of tempo-oxidized cellulose nanofibril films by positron annihilation lifetime spectroscopy. *Biomacromolecules* **12**(11), 4057–4062 (2011). http://doi.org/10.1021/bm201079n.
51. T. Benamor, Synthèse et caractérisation de silices mésoporeuses hydrophobes à porosité contrôlée. PhD thesis, Ecole doctorale Jean Henri Lambert (ED 494), Université de Haute Alsace (2011).
52. G. Hayase, K. Kanamori, K. Abe, H. Yano, A. Maeno, H. Kaji, and K. Nakanishi, Polymethylsilsesquioxane-cellulose nanofiber biocomposite aerogels with high thermal insulation, bendability and superhydrophobicity. *ACS Appl. Mater. Interfaces* **6**(12), 9466–9471 (2014).
53. L.W. Hrubesh, and R.W. Pekala, Thermal properties of organic and inorganic aerogels. *J. Mater. Res.* **9**, 731–738 (1994).
54. X. Lu, R. Caps, J. Fricke, C.T. Alviso, and R.W. Pekala, Correlation between structure and thermal conductivity of organic aerogels. *J. Non Cryst. Solids* **188**, 226–234 (1995).
55. S.T. Nguyen, J. Feng, S.K. Ng, J.P.W. Wong, V.B. C. Tan, and H.M. Duong, Advanced thermal insulation and absorption properties of recycled cellulose aerogels. *Colloids Surf. A Physicochem. Eng. Asp.* **445**, 128–134 (2014).
56. J. Cai, S. Liu, J. Feng, S. Kimura, M. Wada, S. Kuga, and L. Zhang, Cellulose-silica nanocomposite aerogels by in situ formation of silica in cellulose gel. *Angew. Chem. Int. Ed.* **51**, 2076–2079 (2012).
57. M.A.B. Meador, E.F. Fabrizio, F. Ilhan, A. Dass, G. Zhang, P. Vassilaras, J.C. Johnston, and N. Leventis, Cross-linking amine-modified silica aerogels with epoxies: Mechanically strong lightweight porous materials. *Chem. Mater.* **17**, 1085–1098 (2005).
58. M.E. Davis, and R.F. Lobo, Zeolite and molecular sieve synthesis. *Chem. Mater.* **4**, 756–768 (1992).
59. S.T. Nguyen, J. Feng, S.K. Ng, J.P.W. Wong, V.B.C. Tan, and H.M. Duong, Advanced thermal insulation and absorption properties of recycled cellulose aerogels.

Colloids Surf. A Physicochem. Eng. Asp. **445**, 128–134 (2014).
60. S. Sequeira, D.V. Evtuguin, and I. Portugal, Preparation and properties of cellulose/silica hybrid composites. *Polym. Compos.* **30**, 1275–1282 (2009).
61. Pyrogel XT-E, http://www.aerogel.com/products/pdf/Pyrogel_XT-E_DS.pdf, (2013).
62. S.J. Gregg, and K.S.W. Sing, *Adsorption, Surface Area and Porosity*, Academic Press: New York (1982).
63. S. Brunauer, P.H. Emmett, and E. Teller, Adsorption of gases in multimolecular layers. *J. Am. Chem. Soc.* **60**, 309 (1938).
64. T.C.F. Silva, Y. Habibi, J.L. Colodette, T. Elder, L.A. Lucia, A fundamental investigation of the micro-architecture and mechanical properties of tempo-oxidized nanofibrillated cellulose (NFC)-based aerogels. *Cellulose* **19**, 1945–1956 (2012).
65. H. Sehaqui, Q. Zhou, and L.A. Berglund, High-porosity aerogels of high specific surface area prepared from nanofibrillated cellulose (NFC). *Compos. Sci. Technol.* **71**, 1593–1599 (2011).
66. L.J. Gibson, and M.F. Ashby, *Cellular Solids Structure and Properties*, 2nd ed., Cambridge University Press (1997).
67. N. Lavoine, I. Desloges, A. Dufresne, and J. Bras, Microfibrillated cellulose—Its barrier properties and applications in cellulosic materials: A review. *Carbohydr. Polym.* **90**, 735–764 (2012).
68. C. Sanchez, and B. Lebeau, Design and properties of hybrid organic–inorganic nanocomposites for photonics. *MRS Bull.* **26**, 377–387 (2001).
69. O. Foussaier, M. Menetrier, J.J. Videau, and E. Duguet, Polydimethylsiloxane-based ORMOSIL microstructure: Correlation with compressive behavior. *Mater. Lett.* **42**, 305–310 (2000).
70. V. Morales-Flórez, J.A. Toledo-Fernández, M. Piñero, N. de la Rosa-Fox, and L. Esquivias, in: *Proc. XI Int. Conf. Physics Non-Crystalline Solids, Rodas, Greece*, p. 337 (2006).
71. S.T. Nguyen, J. Feng, S.K. Ng, J.P.W. Wong, V.B.C. Tan, and H.M. Duong, Advanced thermal insulation and absorption properties of recycled cellulose aerogels. *Colloids Surf. A Physicochem. Eng. Asp.* **445**, 128–134 (2014).
72. D. Massiot, F. Fayon, M. Capron, I. King, S. Le Calvé, B. Alonso, J.O. Durand, B. Bujoli, Z. Gan, and G. Hoatson, Modelling one and two dimensional solid-state NMR spectra. *Magn. Reson. Chem.* **40**(1), 70–76 (2002).
73. D. Salmon, Thermal conductivity of insulations using guarded hot plates, including recent developments and sources of reference materials. *Meas. Sci. Technol.* **12**(12), 89 (2001).
74. H. Simmler, S. Brunner, U. Heinemann, H. Schwab, and K. Kumaran, Vacuum Insulation Panels. Study on VIP-components and panels for service life prediction of VIP in building applications (Subtask A). Rapport Technique (2005).
75. H. Schwab, U. Heinemann, A. Beck, H.P. Ebert, and J. Fricke, Dependence of thermal conductivity on water content in vacuum insulation panels with fumed silica kernels. *J. Therm. Envel. Build. Sci.* **28**(4), 319–326 (2005).
76. D. Quénard, and H. Sallee, Micro-nano porous materials for high performance thermal insulation. *2nd International Symposium on Nanotechnology in Construction BILBA0* (2005).
77. U. Heinemann, Influence of water on the total heat transfer in 'evacuated' insulations. *Int. J. Thermophys.* **29**(2), 735–749 (2008).

